High-order LES benchmarking in confined rotating disk flows

Stéphane Viazzo, Sébastien Poncet, Eric Serre, Anthony Randriamampianina, Patrick Bontoux

HIGH-ORDER LES BENCHMARKING IN CONFINED ROTATING DISK FLOWS

S. Viazzo, S. Poncet*, E. Serre, A. Randriamampianina, P. Bontoux

Laboratoire M2P2, UMR 6181 CNRS – Aix-Marseille Université – Ecole Centrale Marseille
Technopôle Château-Gombert, 38 rue F. Joliot-Curie, 13451 Marseille
*poncet@l3m.univ-mrs.fr / Tel. 04 91 11 85 23 / Fax 04 91 11 85 02

For many years, the M2P2 laboratory develops highly accurate numerical tools devoted to the study of three-dimensional rapidly rotating flows. These enclosed or opened rotating flows simulate conditions found in a large variety of rotating machinery, including centrifugal pumps, air cycle machines, axial thrust bearings or gas turbines. The present work proposes a benchmark of two Large Eddy Simulation (LES) approaches developed recently in the lab: a fourth order compact finite difference code associated with the dynamic subgrid model and a pseudo-spectral one using a spectral vanishing viscosity technique. We focus on the rotor-stator problem, which is a simplified model of the flow inside rocket engines. The two LES codes have been favourably compared to velocity measurements performed at IRPHE using a two-component LDA system in the case of turbulent rotor-stator flows at Reynolds number equal to 0.4 million. A detailed and accurate picture of the flow for understanding the physics as well as for the assessment of turbulence models for rotating disk systems is provided.

I- INTRODUCTION

The flows associated with disks have been the subject of a constant interest because of their relevance for many applications ranging from disk drives used for digital disk storage in computers to automotive disk brakes, and disks to support turbomachinery blades. Besides its primary concern to industrial applications (Owen & Rogers 1989), the rotor-stator problem has also proved a fruitful means of studying turbulence in confined rotating flows.

According to the combination of the rotation speed Ω and the interdisk spacing h, the present study concerns a flow with two boundary layers separated by a central inviscid rotating core, known as a Batchelor-like flow. Experiments of Itoh $et\ al.$ (1992) have revealed that transition to turbulence first appears within the Bödewadt layer on the stator, even though the flow remains laminar in the Ekman layer along the rotor. They reported a turbulent regime occurring along the stator side at $Re_r = \Omega r^2 / \nu$ $= 8 \times 10^3$ (r the local radius and ν the fluid kinematic viscosity), while along the rotor side, turbulent flow develops later for $3.6 \times 10^5 < Re_r < 6.4 \times 10^5$. Figure 1 shows some flow visualizations performed at IRPHE from above the stator for two Reynolds numbers. A transition to a kind of wave turbulence (Cros $et\ al.$ 2005) is observed for $Re=41000$ and the stator boundary layer becomes fully turbulent for $Re=10^5$.

Differences in turbulence characteristics between the rotor and stator sides have also been observed and attributed to the effects of the radial convective transport of turbulence. As a consequence of confinement, flow curvature and rotation effects, the turbulence is strongly inhomogeneous and anisotropic. Moreover, though the geometry is strictly axisymmetric in cylindrical rotor-stator cavities, the experiments of Czarny $et\ al.$ (2002) revealed the presence of precessing large scale vortical structures even in the turbulent regime, which has been recently confirmed by the URANS computations of Craft $et\ al.$ (2008). These structures may explain the difficulties of bidimensional steady calculations in predicting the flow in disk arrangements (Owen 2000).

The structure of these flows is then highly complex involving laminar, transitional and turbulent flow regions and so these flows are very challenging for turbulence modelling which is today the only numerical approach able to investigate turbulent flows under industrial conditions. The turbulence model must be able to solve the region of low Reynolds number not only near the disks but also in the core of the flow. Moreover, the model has to predict precisely the location of the transition from the laminar to

the turbulent regime, even though the transition process is bounded by instabilities, and so cannot be completely represented by a steady flow model. One of the most important failures of eddy viscosity models in predicting this type of flow is an overestimate of the extent of the relaminarized zone on the inner part of the rotating disk (Iacovides & Theofanoupolos, 1991) leading to erroneous Ekman layer predictions and the rotation rates in the central core. Second moment closures provide a more appropriate level of modelling to predict such complex flows (Launder & Tselepidakis, 1994; Poncet *et al.*, 2005b), but even if they provide a correct distribution of laminar and turbulent regions, the Reynolds stress behaviour is not fully satisfactory, particularly near the rotating disk.
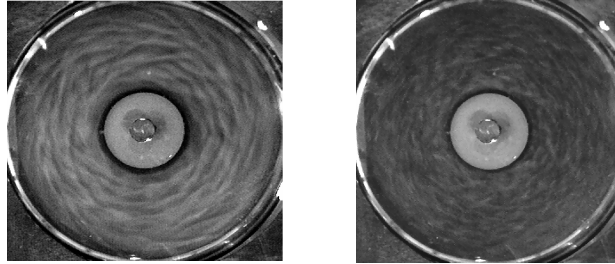

Figure 1: Flow visualizations from above the stator for (a) Re=4.1×10^4 and (b) Re=10^5.

Consequently, the LES seems the appropriate level of modelling. Wu & Squires (2000) performed the first LES of the three-dimensional turbulent boundary-layer over a free rotating disk at Re = 6.5×10^5 and in an otherwise quiescent incompressible fluid using periodic boundary conditions both in the radial and tangential directions. They compared three subgrid-scale (SGS) models: the dynamic eddy viscosity model of Germano *et al.* (1991), the dynamic mixed model of Zang *et al.* (1993), and the dynamic mixed model of Vreman *et al.* (1994). Predictions from six cases were presented to study the effects of grid resolution and SGS model. When the resolution is in a range in which large-scale motions are accurately and well-resolved, Wu & Squires (2000) found no significant effect of both the SGS model and further grid refinement on LES predictions. Compared with previous measurements, the maximum errors in the predicted mean tangential and radial velocities using dynamic models are 4% and 2% of the disk speed, respectively. Good agreement was also obtained between the predicted and measured turbulence intensities. Andersson & Lygren (2006) performed LES of the axisymmetric and statistically steady turbulent flow in an angular section of a rotor-stator cavity for Reynolds numbers ranging from Re = 4×10^5 to Re = 1.6×10^6. They considered five aspect ratios including wide- and narrow-gap disk clearances. They used the mixed dynamic subgrid scale model of Vreman *et al.* (1994). They showed in a previous work (Lygren & Andersson 2004) that this model provided better overall results compared to the dynamic subgrid scale model of Lilly (1992). Finally, Séverac & Serre (2007) proposed a LES approach based on a spectral vanishing viscosity (SVV) technique, which has been applied and validated by Séverac *et al.* (2007) in an enclosed rotor-stator cavity including confinement effects and for Reynolds numbers up to one million.

The turbulent regime is investigated here in a closed annular rotor-stator cavity, using two Large Eddy Simulations. First geometrical and numerical modellings are described in Sections II and III respectively. Comparisons between the LES calculations and previous velocity measurements are performed for a given Reynolds number Re=4×10^5 in Section IV for the mean and turbulent fields. Finally some conclusions and closing remarks are provided in Section V.

II- GEOMETRICAL MODELLING

The cavity shown in Figure 2 is composed by two parallel disks of radius b=140mm, one rotating at a uniform angular velocity Ω (rotor), one being at rest (stator). The disks are delimited by an inner cylinder (the hub) of radius a=40 mm attached to the rotor and by an outer stationary casing (the shroud) attached to the stator. The interdisk spacing, denoted h, is fixed here to 20 mm.
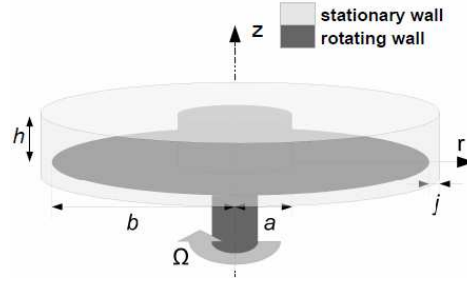
Figure 2: Rotor-stator cavity with relevant notations.

The mean flow is governed by three main control parameters: the aspect ratio of the cavity G, the curvature parameter R_m and the rotational Reynolds number Re based on the outer radius b of the rotating disk defined as follows:

$$G = \frac{b-a}{h} = 5 \qquad R_m = \frac{b+a}{b-a} = 1.8 \qquad Re = \frac{\Omega b^2}{\nu} = 4 \times 10^5$$

where ν is the fluid kinematic viscosity. The values of the geometrical parameters were chosen in order to be relevant with industrial devices such as real stage of turbopump, and to satisfy technical constraints of the IRPHE's device as well as computational effort to reach statistically converged stages. In the experimental setup, a small clearance j=0.85 mm exists between the rotor and the shroud because of mechanical constraints. In the following, the stator is located at $z^*=z/h$=1 and the rotor at z^*=0. We define also the dimensionless radial location as $r^*=(r-a)/(b-a)$.

III- NUMERICAL APPROACHES

The incompressible fluid motion is governed by the three-dimensional Navier-Stokes equations written in primitive variables for cylindrical coordinates (r,θ,z). They are solved using two different Large Eddy Simulation (LES) codes: a fourth order compact finite difference code associated with the dynamic subgrid model, denoted LES-FD in the following and a pseudo-spectral one using a spectral vanishing viscosity approach, and denoted LES-SVV.

LES-FD

In the LES-FD code, each variable of the flow is split into a computed large anisotropic scale component and a small scale component called subgrid-scale, which is more isotropic and universal and has to be modeled. This separation is obtained by applying a spatial filter to the Navier–Stokes and continuity equations in order to reduce the amount of spatial scales to be solved. The subgrid scale stress τ_{ij} is expressed using the Leonard decomposition. The complex interactions between the resolved and unresolved scales are modelled using a turbulent eddy viscosity hypothesis. The anisotropic part of the subgrid scale stress τ_{ij} is linked to the eddy viscosity ν_T by the following expression:

$$\tau_{ij} - \frac{\delta_{ij}}{3}\tau_{kk} = -2\nu_T \overline{S}_{ij} \text{ with } \nu_T = C\overline{\Delta}^2|\overline{S}| \text{ and } |\overline{S}| = \sqrt{2\overline{S}_{ij}\overline{S}_{ij}} \tag{1}$$

where C is the dimensionless model coefficient, $\overline{\Delta} = (\Delta_r\Delta_\theta\Delta_z)^{1/3}$ the grid filter width and S_{ij} the strain rate tensor. This classical Smagorinsky model was tested as a first approach but it appears too dissipative. Furthermore, it does not allow possible subgrid scale energy backscatter to the resolved scales. The dynamic Smagorinsky model which overcomes some of the drawbacks of the Smagorinsky model is a suitable alternative. Initially developed by Germano *et al.* (1991) to correct the excessive

dissipation of the Smagorinsky model and modified by Lilly (1992), this model exhibits the correct asymptotic behavior near the walls and in laminar regions, and does not normally prohibit possible energy backscatter. The square of the constant C_s^2 is replaced by a coefficient C_d which is dynamically computed and depends on the local structure of the flow. In order to compute C_d, a test filter denoted by a hat with a width larger than the grid filter is introduced. The dynamic constant is calculated with a least-squares approach according to:

$$C_d = -\frac{1}{2}\frac{(L_{ij}-L_{kk}\delta_{ij}/3)M_{ij}}{M_{ij}M_{ij}}$$ (2)

$$L_{ij} = \overline{\hat{\overline{u_i}\,\overline{u}_j}} - \hat{\overline{u}}_i\hat{\overline{u}}_j$$ (3)

$$M_{ij} = \hat{\overline{\Delta}}^2\left|\hat{\overline{S}}\right|\hat{\overline{S}}_{ij} - \overline{\Delta}^2\widehat{\left|\overline{S}\right|\overline{S}_{ij}}$$ (4)

The model coefficient C_d which is dynamically computed is a local and instantaneous quantity and thus can vary widely in time and space. However, this desirable property may lead to numerical instabilities caused by negative values of C_d. Accordingly, the numerator and denominator of Equation (2) are averaged in the homogeneous tangential direction. Furthermore, negative values of ν_T are clipped to zero if the turbulent viscosity ν_T is negative. The test filter used in the dynamic Smagorinsky model is a symmetric discrete filter based on the trapezoidal rule:

$$\hat{f}_i = \frac{1}{4}(f_{i-1} + 2f_i + f_{i+1})$$ (5)

This filter is applied sequentially in each non homogeneous direction. The cutoff filter is applied in the azimuthal direction. The value of the ratio $\hat{\overline{\Delta}}/\overline{\Delta}$ is fixed to 2.

Schiestel and Viazzo (1995) have previously found that non-staggered grids cannot prevent oscillatory numerical wiggles in the pressure field. In order to circumvent the pressure checkerboarding, a staggered MAC mesh is used. The convective terms are considered in the skew-symmetric form since their discrete analogues preserve the global conservation of momentum and kinetic energy on staggered mesh (in the inviscid limit). The spatial discretization is based on fourth order compact schemes in the inhomogeneous radial and axial directions whereas Fourier pseudospectral methods are appropriate in the homogeneous tangential direction. The time advancement is second order accurate and is based on the explicit Adams–Bashforth scheme for the convective terms and the implicit Crank–Nicolson scheme for the viscous terms. The system of equations is solved using a two-step fractional scheme (predictor– corrector). At each time step, the problem reduces to a set of three Helmholtz equations (for the velocity components) and two Poisson equations (for the preliminary pressure and the pressure correction). The eddy viscosity depends both on time and space, so internal iterations are necessary for the resolution of the predictor step. Practically, five iterations are required to obtain a convergence criterion of 10^{-6}. In the radial and axial directions, the grid is non uniform using hyperbolic tangent transformations, whereas in the azimuthal periodic direction the distribution is uniform. The number of grid points is 120x65x192 respectively in the radial, axial and azimuthal directions. The time step is 5.10^{-6} s.

LES-SVV

The pseudospectral numerical method is based on a collocation-Chebyshev method in the r and z inhomogeneous directions and a Galerkin-Fourier method in the azimuthal periodic direction θ. Thus, each dependent variable $f = (V_r, V_\theta, V_z, p)$ is expanded into a truncated trigonometric series:

$$f_{NMK}(r,\theta,z,t) = \sum_{n=0}^{N-1} \sum_{m=0}^{M-1} \sum_{k=-K/2}^{K/2-1} \hat{f}_{nmk}(t)\, T_n(r)\, T_m(z)\, e^{ik\theta} \tag{6}$$

where T_n and T_m are Chebyshev polynomials of degrees n and m, respectively. N and M define the number of collocation points in the radial and axial directions, respectively, and K is the cutoff in the tangential direction. To ensure high accuracy of the solution within the very thin wall layers, this approximation is applied at the Gauss-Lobatto collocation points, where the differential equations are assumed to be satisfied exactly, defined as $r_i = \cos(i\pi/N)$ for $i \in [0,N]$ and $z_j = \cos(j\pi/M)$ for $j \in [0,M]$ in the radial and axial directions. In the azimuthal direction, an uniform distribution is considered: $\theta_k = 2k/K$ for $k \in [0,K]$.

The temporal discretization is a projection scheme, based on backwards differencing in time (see all the details in Raspo *et al.* 2002). The specificity of the algorithm is to allow a temporal evolution of the normal pressure gradient at the boundaries. The temporal scheme is second-order semi-implicit combining an implicit second order backward Euler scheme for the diffusive terms and an explicit Adams-Bashforth extrapolation for the non-linear convective terms. For each Fourier mode, a full diagonalization technique is used for solving a set of 2D uncoupled Helmholtz and Poisson problems obtained after splitting the Euler scheme to group the implicit part in the left hand side of the equations.

The LES is performed through a Spectral Vanishing Viscosity technique (SVV) (Karamanos & Karniadakis 2000, Pasquetti & Xu 2002, Séverac & Serre 2007). In the frame of collocation method, an appropriate viscosity kernel operator is incorporated in the Helmholtz equations of velocity prediction, only active for high wave numbers of the numerical approximation. This operator does not affect the large scales of the flow and stabilise the solution by increasing the dissipation, particularly near the cut off frequency. According to Karamanos & Karniadakis (2000), we choose to define our SVV operator, written in 1D as follows:

$$\nu \Delta_{SVV} v_N = \nu \Delta v_N + \varepsilon_N\, \partial_x \left(Q_N \frac{\partial v_N}{\partial x} \right) \tag{7}$$

where v_N is the velocity vector approximation and Q_N is the 1D kernel operator defined in spectral space as a C^∞ smooth function:

$$\hat{Q}_N(\omega_n) = 0 \quad \text{for} \ 0 \leqslant \omega_n \leqslant \omega_T \tag{8}$$

$$\hat{Q}_N(\omega_n) = \varepsilon_N e^{-[(\omega_N-\omega_n)/(\omega_T-\omega_n)]^2} \quad \text{for} \ \omega_T \leqslant \omega_n \leqslant \omega_N \tag{9}$$

The 3D SVV operator Q_N is composed of three 1D SVV operators $Q_{N_i}^i$; i=1, 2, 3 corresponding to the (r, θ, z) directions respectively; the operator is parameterized by $\varepsilon_{N_i}^i$ the maximum of viscosity and ω_T^i the threshold after which, the viscosity is applied. ω_N^i is the highest frequency calculated in the direction i. Because our SVV operator is fully linear, it is gathered with the implicit standard diffusion term. Consequently, no additional computational cost is needed. Another advantage is that the SVV operator affects at most two-thirds of the spectrum on the highest frequencies (ω_T=0) and so, DNS results are easily recovered for laminar flows. The reader is referred to the previous paper of Séverac & Serre (2007) for more details about the LES-SVV numerical modelling. The computational parameters used in the present LES-SVV are summed up in table 1, where δt is the time step.

direction	ω_T	ε_N	Grid	δt (s)
r	$0.8\,N^{1/2}$	$1/(2N)$	N=121	
θ	$N^{1/2}$	$1/(2N)$	K=181	$2\pi\,10^{-4}$
z	$N^{1/2}$	$1/(2N)$	M=65	

Table 1: Computational parameters for the LES-SVV code

For both LES approaches, no-slip boundary conditions are applied at all walls. The tangential velocity is fixed to 0 on the stator and on the shroud and to the local disk velocity on the rotor and the hub. The singularities present in the experiments at the junctions between rotating and stationary walls are regularized in the two LES codes by using an exponential function to provide a smooth switchover. The calculated quantities have been averaged both in time and in the tangential direction.

IV- COMPARISONS BETWEEN THE LES APPROACHES

The two LES approaches are compared to velocity measurements performed at IRPHE using a two component laser Doppler anemometer (LDA) from above the stator. About 5000 validated data are necessary to obtain the statistical convergence of the measurements. The mean and turbulent quantities are given with an accuracy of 2 and 5% respectively. Comparisons with the Reynolds Stress Modelling (RSM) of Elena & Schiestel (1995) are also provided. This model has been sensitized to the implicit effects of rotation on turbulence and applied to a wide range of flow conditions in enclosed or opened rotor-stator cavities (Poncet *et al.* 2005b).
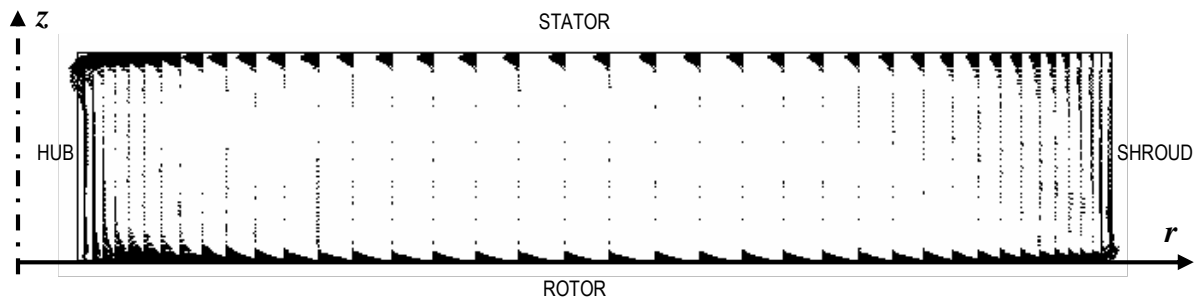

Figure 3: Instantaneous velocity vector field in a (*r*,*z*) plane obtained by the LES-FD code.

On average, the base flow in a rotor-stator cavity is axisymmetric and three-dimensional due to the circulation in the meridional plane created by the centrifugal force associated with a tangential main flow due to the rotation of the disk. The secondary flow in a (*r*,*z*) plane is shown in Figure 3 from the instantaneous velocity vector field. In this plane, the flow is broadly a Batchelor flow with two boundary layers developed on each disk separated by a central rotating core. There is no axial gradient in the core as a consequence of the Taylor-Proudman theorem. Its secondary flow is essential radial within the boundary layers: the fluid is pumped centrifugally outwards along the rotor and is deflected in the axial direction after impingement on the external cylinder. After a second impingement on the stator, it flows radially inwards along the stator, by conservation of mass, before turning along the hub and being centrifuged again by the rotating disk. The main effect of finite-radius disks and most of all of the inner and outer cylinders is that the boundary conditions are not compatible with self-similarity solutions though there may be qualitative resemblance far from the end walls. Thus, the thicknesses of the Ekman layer on the rotor and of the Bödewadt layer on the stator are not constant along the radius within the cavity. Note that the Bödewadt layer is almost twice thicker than the Ekman layer.

Figure 4 presents the axial profiles of the mean radial $V_r^*=V_r/(\Omega r)$ and tangential $V_\theta^*=V_\theta/(\Omega r)$ velocity components at mid-radius $r^*=0.5$. The axial profile of the mean axial velocity component is not shown here because we recall that it is quasi equal to zero far from the inner and outer cylinders. The LES-FD and LES-SVV are compared to both LDA measurements and the predictions of the RSM model. From the V_θ^*-profile, we can clearly see that the mean flow exhibits a Batchelor-like flow structure, with two boundary layers separated by a core in solid body rotation. The crucial quantity for engineering applications is the entrainment coefficient of the fluid or the core swirl ratio because it is directly linked to the radial pressure gradient in the cavity and as a consequence to the axial thrusts applied on the rotor (Poncet *et al.* 2005a). This coefficient is usually denoted *K* and defined as the ratio

between the tangential velocity of the fluid in the core and the local disk velocity at the same radius. The LES-SVV and LES-FD computations predict K equal to 0.36 and 0.32 respectively for $Re=4\times10^5$ at $r^*=0.5$, which is to be compared to the measured value $K=0.36$ and to the value $K=0.315$ predicted by the RSM. All these values fall between the laminar similarity solution $K=0.313$ obtained numerically by Pearson (1965) for infinite-disk cavities, and the asymptotic value $K=0.43$ of Poncet *et al.* (2005a) deduced from their analytical model for highly turbulent flows. The low value of K found in the four approaches together with the local extrema of V_θ^* at the edge of the boundary layers are typical of the transitional regime with a relatively low level of turbulence.
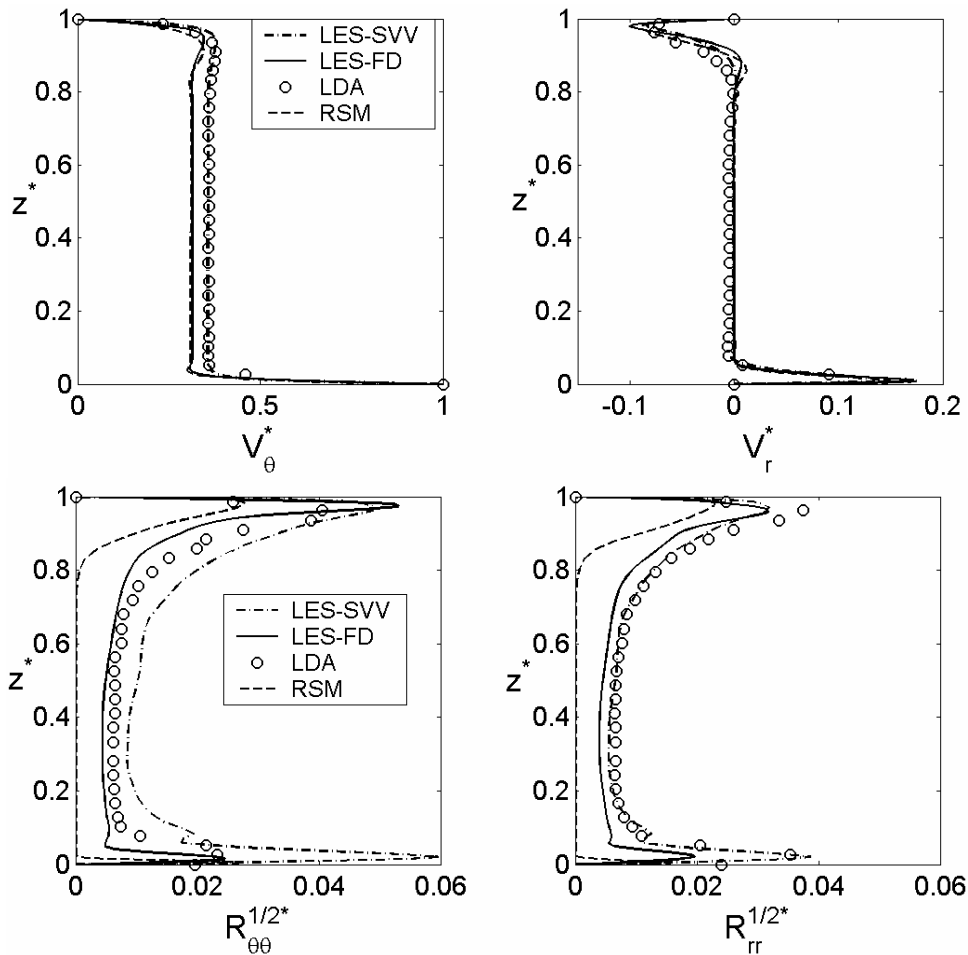

Figure 4: Axial profiles of the mean tangential and radial velocity components and of the two main Reynolds stress tensor components at $r^*=0.5$. Comparisons between the LES-SVV (-·-), the LES-FD (—), the LDA measurements (o) and the RSM model (- -).

The LES-SVV and LES-FD predict quite well the thickness of the Ekman layer on the rotor, which scales like $\delta=(\nu / \Omega)^{1/2}$, which is the thickness of the boundary layer over a single rotating disk. The LES-SVV slightly underestimates the thickness of the Bödewadt layer but provides better overall results than the LES-FD and the RSM. The V_r^*-profile deduced from the RSM model exhibits a local extremum around $z^*=0.8$. This local extremum together with the underestimation of the coefficient K are typical of an underestimation of the turbulence intensities. The agreement between the LES-FD and LES-SVV results and the measurements is quite satisfactory for the mean field. Both LES catch relatively well the main features of turbulent rotor-stator flows such as the entrainment coefficient K and the thicknesses of the boundary layers.

The axial profiles of the two main normal Reynolds stress tensor components $R_{rr} = \overline{v_r'^2}/(\Omega r)^2$ and $R_{\theta\theta} = \overline{v_\theta'^2}/(\Omega r)^2$ are shown at mid-radius in Figure 4. It corresponds to a local Reynolds number Re_r=1.65×10⁵, for which the stator boundary layer is turbulent, whereas the rotor one is still laminar according to the experiments of Itoh *et al.* (1992). These authors found indeed that the rotating layer becomes turbulent for Re_r = 3.6×10⁵. From the two LES and the LDA data, both boundary layers are turbulent at this radius, whereas the core remains laminar. The turbulence intensities are larger on the rotor than on the stator in the LES-SVV results, which is not the case for the LES-FD. The numerical profiles from the two LES codes fit quite well the experimental measurements both in the boundary layers and in the core. Let's notice however, that the agreement between the maxima in stator layer is less satisfying, with LES values smaller (respectively larger) in the radial direction (respectively in the tangential direction) than the experimental data. As a consequence, the anisotropy of the normal stresses is stronger in LES than in experiment. The location of the normal stresses maxima is relatively well predicted within the stator layer for both radial and tangential directions; at a distance from the stator equal to 0.05*h* for the radial component and two times closer 0.025*h* for the tangential component. Note that the experimental values of the $R_{r\theta}^*$ component are very close to zero (not represented here), whereas the LES codes predict a strong shear stress in both boundary layers. The tendency of the RSM is a too high relaminarization of the flow in the Bödewadt layer and in the core. It predicts also a laminar Ekman layer, which is in agreement with the results of Itoh *et al.* (1992).
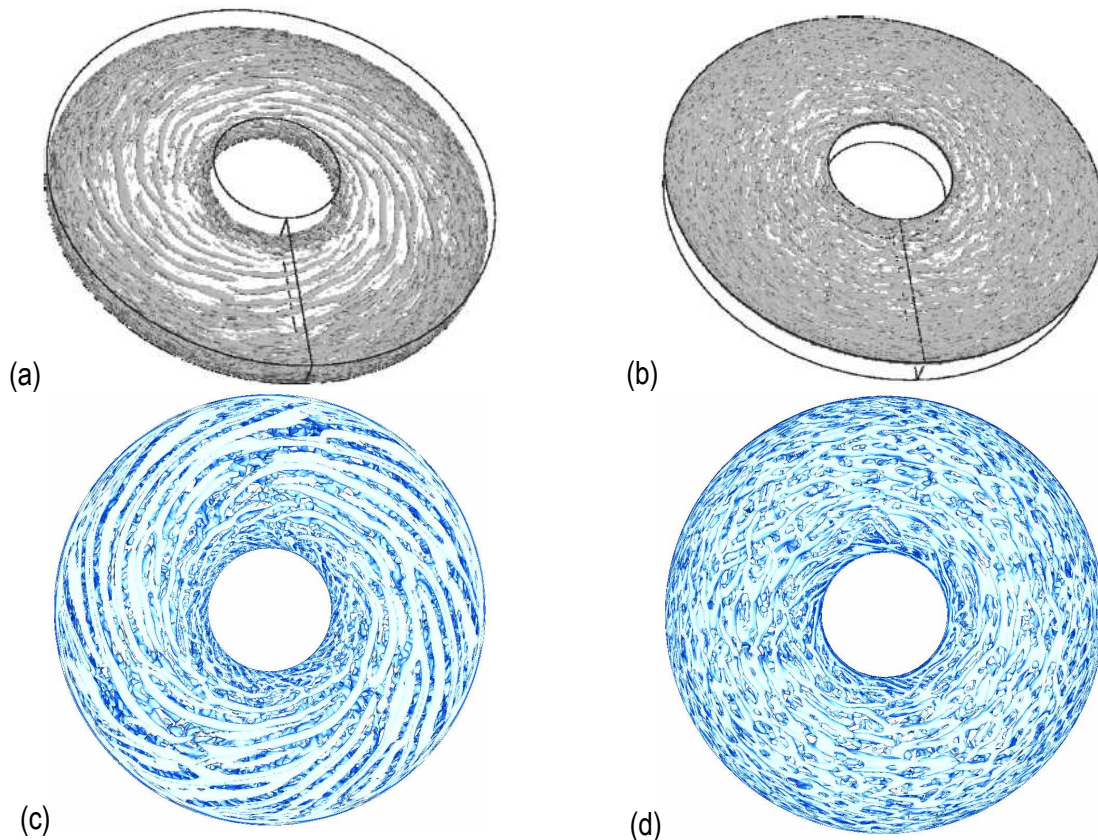

(a)   (b)

(c)   (d)

Figure 5: Iso-surfaces of the Q-criterium along the rotor (a,c) and along the stator (b,d) obtained by the LES-SVV code (a,b) and by the LES-FD code (c,d). The rotating disk rotates counterclockwise.

Figure 5 presents the iso-values of the Q-criterium along both disks obtained by the two LES approaches. At this Reynolds number Re=4×10⁵, the rotating disk layer is transitional with positive spiral arms (as they roll up in the rotation sense of the disk) at intermediate radii and more thin turbulent structures along the hub where the flow coming from the Bödewadt layer impinges the rotor (Fig.3).

From the LES-SVV, 19 spiral arms (Fig.5a) forming a positive angle ε =16° with the tangential direction appear in the Ekman layer for $0.14 \leq r^* \leq 0.61$, where the flow is laminar unstable $89 \leq Re_r^{1/2} \leq 386$. These structures are characteristic of the Type I instability (cross-flow instability), which plays an important role in the transition process to turbulence. The same large spiral arms are obtained by the LES-FD (Fig.5c) characterized by the same azimuthal wave number and the same angle. A small difference is observed along the external cylinder, where the spirals are still visible in the LES-FD, whereas the LES-SVV predicts more thin axisymmetric structures typical of highest turbulence levels. Along the stationary disk, both LES exhibit very thin coherent vortical structures aligned with the tangential direction (Fig.5b,d).

V- CONCLUSION

A numerical investigation of the turbulent flow in a shrouded rotor-stator cavity has been performed by two LES codes for a Reynolds number equal to $Re=4×10^5$. The highly accurate computation of turbulent rotating flows within cavity is of interest for both engineering applications with turbomachinaries, and also fundamental research. The first LES approach, denoted LES-SVV, is a 3D spectral code stabilized with a Spectral Vanishing Viscosity model, whereas the second one, denoted LES-FD, is a fourth order compact finite difference code associated with the dynamic subgrid model. The LES-SVV and LES-FD computations compared quite favourably with previous LDA measurements, which is very encouraging for these numerical approaches to deal with complex flows. In the same time, the second order RSM model tends to relaminarize the flow.

The LES-SVV provides better overall results compared to the LES-FD but no definitive conclusion can be drawn from these preliminary results. More computations are now required and especially at higher Reynolds numbers to study the influence of the SGS model on the turbulence structure in a highly turbulent flow. Improvements in the future for the LES-SVV should come from a coupling of the SVV procedure to the flow dynamics in order to optimize the dissipation of the model. Computations performed using a third LES code based on a pseudo-spectral method associated with the dynamic subgrid model are also in progress to complete this benchmark.

REFERENCES

Andersson H.I., Lygren M. 2006. LES of open rotor-stator flow, *Int. J. Heat Fluid Flow* **27**, p.551-557.
Craft T., Iacovides H., Launder B.E., Zacharos A. 2008. Some swirling-flow challenges for turbulent CFD, *Flow, Turbulence & Combustion* **80**, p.419-434.
Cros A., Floriani E., Le Gal P., Lima R. 2005. Transition to turbulence of the Batchelor flow in a rotor/stator device. *Eur.J. Mech.B/Fluids* **24**, p.409-424.
Czarny O., Iacovides H., Launder B.E. 2002. Precessing vortex structures in turbulent flow within rotor-stator disc cavities, *Flow, Turbulence & Combustion* **69**, p.51-61.
Elena L., Schiestel R. 1995. Turbulence modeling of confined flow in rotating disk systems, *AIAA J.* **33 (5)**, p.812-821.
Germano M., Piomelli U., Moin P., Cabot W.H. 1991. A dynamic subgrid-scale eddy viscosity model, *Phys. Fluids A* **3(7)**, p.1760-1765.
Iacovides H., Theofanoupolos I.P. 1991. Turbulence modelling of axisymmetric flow inside rotating cavities, *Int. J. Heat Fluid Flow* **12**, p.2-11.
Itoh M., Yamada Y., Imao S., Gonda M. 1992. Experiments on turbulent flow due to an enclosed rotating disc, *Exp. Thermal*

Fluid Sci. **5**, p.359-368.

Karamanos G.S., Karniadakis G.E. 2000. A spectral vanishing viscosity method for large eddy simulation, *J. Comp. Phys.* **163**, p.22-50.

Launder B.E., Tselepidakis, D.P. 1994. Application of a new second moment closure to turbulent channel flow rotating in orthogonal mode, *Int. J. Heat Fluid Flow* **15**, pp.2-10.

Lilly D.K. 1992. A proposed modification of the Germano subgrid-scale closure method. *Phys. Fluids A* **4**, p.633–635.

Lygren M., Andersson H. 2004. Large eddy simulation of the turbulent flow between a rotating and a stationary disk, *ZAMM* **55**, p.268-281.

Owen J. M. 2000. Flow and heat transfer in rotating-disc systems*, CHT01 Turbulence, Heat & Mass Transfer*, Ed. Y. Nagano, K. Hanjalic, T. Tsuji, Aichi Shuppan Press, p.33-58.

Owen J. M., Rogers R.H. 1989. *Flow and heat transfer in rotating-disc systems, Vol. 1: Rotor-stator sytems*, Research Studies Press, Taunton.

Pasquetti R., Xu C.J. 2002. High-order algorithms for large-eddy simulation of incompressible flows, *J. of Sci. Comp.* **17**, p.273-284.

Pearson CE. 1965. Numerical solutions for the time-dependent viscous flow between two rotating coaxial disks. *J. Fluid Mech.* **21 (4)**, p.623-33.

Poncet S., Chauve M.-P., Le Gal P. 2005a. Turbulent Rotating Disk Flow with Inward Throughflow, *J. Fluid Mech.*, **522**, p.253-262.

Poncet S., Chauve M.-P., Schiestel R. 2005b. Batchelor versus Stewartson flow structures in a rotor-stator cavity with throughflow, *Phys. Fluids* **17**, 075110.

Raspo I., Hugues S., Serre E., Randriamampianina A., Bontoux P. 2002. Spectral projection methods for the simulation of complex three-dimensional rotating flows, *Computers and Fluids* **31**, p.745-767.

Schiestel R., Viazzo S. 1995. A Hermitian–Fourier numerical method for solving the incompressible Navier–Stokes equations. *Comput. Fluids* **24**, p. 739–752.

Séverac E., Serre E. 2007. A spectral vanishing viscosity for the LES of turbulent flows within rotating cavities, *J. Comp. Phys.* **226 (2)**, p.1234-1255.

Séverac E., Poncet S., Serre E., Chauve M.-P. 2007. Large eddy simulation and measurements of turbulent enclosed rotor-stator flows, *Phys. Fluids* **19**, 085113.

Vreman B., Geurts B., Kuerten H. 1994. On the formulation of the dynamic mixed subgrid-scale model. *Phys. Fluids* **6**, p.4057–4059.

Wu X., Squires K.D. 2000. Prediction and investigation of the turbulent flow over a rotating disk, *J. Fluid. Mech.* **418**, p.231-264.

Zang Y., Street R., Koseff J.R. 1993. A dynamic mixed subgrid-scale model and its application to turbulent recirculating flows, *Phys. Fluids* **5(12)**, p.3186-3196.